Four-neutrino oscillation solutions of the atmospheric neutrino anomaly

G. L. Fogli, E. Lisi, and A. Marrone
Dipartimento di Fisica and Sezione INFN di Bari, Via Amendola 173, I-70126 Bari, Italy
(Received 2 October 2000; published 7 February 2001)

In the context of neutrino scenarios characterized by four (three active plus one sterile) neutrino species and by mass spectra with two separated doublets, we analyze solutions to the atmospheric neutrino anomaly which smoothly interpolate between $\nu_\mu \to \nu_\tau$ and $\nu_\mu \to \nu_s$ oscillations. We show that, although the Super-Kamiokande data disfavor the *pure* $\nu_\mu \to \nu_s$ channel, they do not exclude its occurrence, with sizable amplitude, *in addition* to the $\nu_\mu \to \nu_\tau$ channel. High energy muon data appear to be crucial in assessing the relative amplitude of active and sterile neutrino oscillations. It is also qualitatively shown that such atmospheric ν solutions are compatible with analogous solutions to the solar neutrino problem, which involve oscillations of ν_e in both sterile and active states.

DOI: 10.1103/PhysRevD.63.053008 PACS number(s): 14.60.Pq, 13.15.+g, 95.85.Ry

I. INTRODUCTION

Four-neutrino (4ν) models, involving the three known active states (ν_e, ν_μ, ν_τ) plus one hypothetical sterile state (ν_s), are being intensively studied in the context of the current neutrino phenomenology, since they can accommodate (through three independent mass square differences) the three sources of evidence for ν flavor oscillations coming from atmospheric, solar, and accelerator neutrino experiments. In particular, 4ν spectra with mass eigenstates organized in two doublets (2+2 models) seem to be favored by world neutrino data [1]. Updated reviews on such 4ν models and on their phenomenology can be found, e.g., in [2–4], to which the reader is referred for an extended bibliography and for details that are not repeated in this work.

According to the conventional wisdom, 2+2 models are often assumed to imply, for the solar and atmospheric oscillation channels, either

$$\nu_\mu \to \nu_\tau \quad \text{(atmospheric)}, \tag{1a}$$

$$\nu_e \to \nu_s \quad \text{(solar)}, \tag{1b}$$

or

$$\nu_\mu \to \nu_s \quad \text{(atmospheric)}, \tag{2a}$$

$$\nu_e \to \nu_\tau \quad \text{(solar)}, \tag{2b}$$

in addition to inter-doublet $\nu_\mu \to \nu_e$ oscillations with small amplitude, required to explain the Liquid Scintillator Neutrino Detector (LSND) signal [5,6].

Such simplifying assumptions are challenged by the recent Super-Kamiokande (SK) observations, which tend to disfavor (dominant) oscillations into ν_s of both atmospheric muon neutrinos (at $\sim$99% C.L. [7,8]) and solar electron neutrinos (at $\sim$95% C.L., in combination with world solar ν data [9]). The MACRO experiment also disfavors atmospheric $\nu_\mu \to \nu_s$ oscillations (at $\sim$95% C.L. [10]). However, it seems premature to rule out the sterile neutrino hypothesis on the basis of the present information only [11,12]: on the one hand, past experience on global data fits has shown that, sometimes, hypotheses rejected (accepted) at 95% or 99% C.L. can surprisingly revive (die); on the other hand, the underlying 4ν oscillation pattern might be more complicated [3,13,14] than assumed in Eqs. (1a),(1b) or (2a),(2b). In particular, instead of having decoupled active and sterile oscillation channels, one might have mixed (active+sterile) flavor transitions of the kind [15]

$$\nu_\mu \to \nu_+ \quad \text{(atmospheric)}, \tag{3a}$$

$$\nu_e \to \nu_- \quad \text{(solar)}, \tag{3b}$$

where the states $\nu_\pm$, as discussed later in more detail, represent linear (orthogonal) combinations of ν_τ and ν_s through a mixing angle ξ,

$$\nu_+ = +\cos\xi\,\nu_\tau + \sin\xi\,\nu_s, \tag{4a}$$

$$\nu_- = -\sin\xi\,\nu_\tau + \cos\xi\,\nu_s. \tag{4b}$$

The oscillation modes (3a),(3b) represent generalizations of both modes (1a),(1b) and (2a),(2b), to which they reduce for $\sin\xi = 0$ and 1, respectively. For generic values of $\sin\xi$, the final states in atmospheric ν_μ and solar ν_e flavor transitions are linear combinations of ν_s and ν_τ, with coefficients to be constrained by experiments.

In this work, we quantitatively study atmospheric four-neutrino oscillations in the context of 2+2 spectra, for unconstrained values of $\sin\xi = \langle \nu_+ | \nu_s \rangle$. It is shown that the state ν_+ (into which ν_μ oscillates) can have a sizable ν_s component, which is testable through high-energy atmospheric muon data. Our atmospheric ν results are also qualitatively compared with recent 4ν solutions to the solar neutrino problem [13,14], which are compatible with a large ν_s component of ν_-. It is shown that both solar and atmospheric neutrino oscillations are consistent with sizable flavor transitions to a sterile state.

The structure of this paper is as follows. In Sec. II we introduce the theoretical 4ν framework, and in Sec. III we show the corresponding graphical representation of the parameter space. Section IV reports a preliminary discussion of the SK experimental information, while Sec. V is devoted to

a thorough SK atmospheric ν data analysis, from which we derive constraints on 4ν mass-mixing parameters. Their consistency with solar neutrino data is discussed in Sec. VI. Remarks on alternative 4ν scenarios are made in Sec. VII. Finally, conclusions and perspectives are reported in Sec. VIII.

While this work was being completed, our attention was brought to the paper [16], where 4ν solutions to the atmospheric neutrino anomaly have also been worked out. The 4ν scenario considered in [16] contains two additional parameters as compared with ours (a mixing angle s_{23} and a CP violation phase δ_1 [16]), and most of the results shown refer to such parameters, so that a direct comparison with our results is difficult. However, we agree with [16] on some general features, namely, that atmospheric ν_μ can have a large transition amplitude to ν_s (in addition to $\nu_\mu \to \nu_\tau$), and that such transitions are consistent with solar neutrino data.

II. THEORETICAL FRAMEWORK

In this section we define the theoretical 4ν framework and the notation used in our analysis. We also motivate a few data-driven assumptions, which considerably simplify both the analysis and the understanding of the solar and atmospheric ν oscillations.

A. General conventions

We order the neutrino flavor and mass eigenstates in column vectors as

$$\nu_\alpha = (\nu_e, \nu_s, \nu_\mu, \nu_\tau)^T, \tag{5}$$

$$\nu_i = (\nu_1, \nu_2, \nu_3, \nu_4)^T, \tag{6}$$

respectively (T=transpose). Such vectors are related by a unitary mixing matrix U,

$$\nu_\alpha = U_{\alpha i} \nu_i . \tag{7}$$

The matrix of squared neutrino masses (in the ν_i basis) is defined as

$$\mathcal{M} = \mathrm{diag}(m_1^2, m_2^2, m_3^2, m_4^2) + \lambda^2 \mathbf{1}, \tag{8}$$

where the term $\lambda^2\mathbf{1}$ reminds that the overall mass scale λ is unconstrained, as far as oscillation experiments are concerned. We define three independent mass square differences, phenomenologically related to the evidence for oscillations coming from solar, atmospheric, and LSND experiments,

$$\delta m^2 = m_2^2 - m_1^2 \ \ (\text{solar}), \tag{9a}$$

$$m^2 = m_4^2 - m_3^2 \ \ (\text{atmos.}), \tag{9b}$$

$$M^2 = m_3^2 - m_2^2 \ \ (\text{LSND}). \tag{9c}$$

With the above definitions, the neutrino evolution equation in the flavor basis,

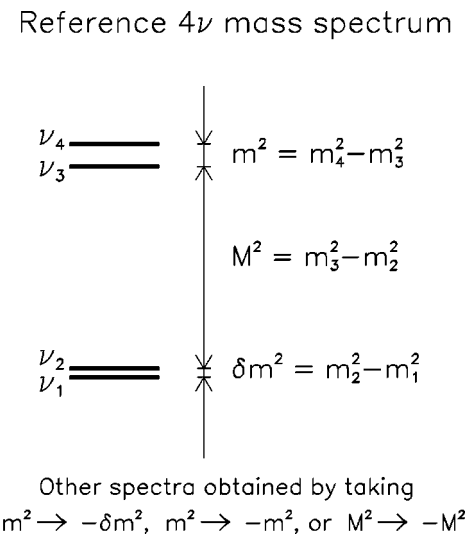

FIG. 1. The reference 4ν mass spectrum adopted in this work.

$$i\frac{d}{dx}\nu_\alpha = \mathcal{H}\nu_\alpha , \tag{10}$$

is governed by the Hamiltonian

$$\mathcal{H} = \frac{1}{2E} U\mathcal{M}U^\dagger + \sqrt{2}G_F \mathrm{diag}\left(N_e, \frac{1}{2}N_n, 0, 0\right), \tag{11}$$

where the first (kinematical) term [17] depends on the neutrino energy E, and the second (dynamical) term [18] depends on the neutrino weak interactions with background electrons (with density N_e) and neutrons (with density N_n) in matter.

B. Approximations concerning 4ν masses and mixing

Motivated by the current 4ν oscillation phenomenology (see [2–4] and references therein), we assume that the mass eigenstates are organized in two doublets (2+2 spectrum),

$$m_1 \simeq m_2 < m_3 \simeq m_4 \tag{12}$$

with three widely different mass squared differences,

$$\delta m^2 \ll m^2 \ll M^2. \tag{13}$$

Figure 1 shows our reference mass spectrum, with a lower ''solar neutrino doublet'' (ν_1, ν_2), and an upper ''atmospheric neutrino doublet'' (ν_3, ν_4), separated by a relatively large LSND mass gap. Other phenomenologically allowed 2+2 spectra can be obtained by interchanging the two doublets ($M^2 \to -M^2$), as well as the two states in a doublet ($\delta m^2 \to -\delta m^2$, or $m^2 \to -m^2$, or both). We anticipate that, under the approximations discussed below, the oscillation physics in such alternative 2+2 spectra is equivalent (under appropriate changes of variables) to that in the spectrum of

Fig. 1. Therefore, our reference choice in Fig. 1 does not represent a limitation, as far as 2+2 spectra are considered.[1] We also anticipate that, under the same approximations, CP violation effects turn out to be unobservably small in current experiments, so that the mixing matrix U can be effectively taken as real,

$$U^\dagger \simeq U^T. \tag{14}$$

Further assumptions about the mixing matrix U can be adopted by comparing positive disappearance results at the mass scale δm^2 (solar $\nu_e \to \nu_e$) and m^2 (atmospheric $\nu_\mu \to \nu_\mu$) with negative disappearance results at the mass scale M^2 in short-baseline accelerators (no $\nu_\mu \to \nu_\mu$) and reactors (no $\nu_e \to \nu_e$) (see, e.g., [3]). Such results imply that the ν_μ component of the atmospheric doublet (ν_3, ν_4) must be large to explain the atmospheric ν_μ anomaly, but must be small in the other doublet (ν_1, ν_2), in order to avoid large M^2-driven $\nu_\mu \to \nu_\mu$ oscillations at short-baseline accelerators. Analogously, the ν_e component of the solar doublet (ν_1, ν_2) must be large to explain the solar ν_e deficit, but it must be small in the other doublet (ν_3, ν_4), in order to avoid large M^2-driven $\nu_e \to \nu_e$ oscillations at reactors. Therefore, one can take

$$U_{\mu 1}^2 + U_{\mu 2}^2 \simeq 0, \tag{15}$$

$$U_{e3}^2 + U_{e4}^2 \simeq 0. \tag{16}$$

Some remarks on the above two assumptions are in order. In 4ν models embedding LSND, Eqs. (15) and (16) must be slightly violated—at the few permill level—in order to get a nonzero value for the small (few permill) LSND $\nu_\mu \to \nu_e$ oscillation amplitude, given by $A_{\rm LSND} = 4|U_{\mu 3}U_{e3} + U_{\mu 4}U_{e4}|^2 = 4|U_{\mu 1}U_{e1} + U_{\mu 2}U_{e2}|^2$ [2–4]. A few permill violation makes little difference in the analysis of current solar and atmospheric neutrino data, and will be neglected in the following. One cannot exclude, however, more general scenarios in which $U_{\mu 1}^2 + U_{\mu 2}^2$ is taken close to the weakest upper limits allowed by accelerators (of the order of ten percent [20]) and can thus play a nonnegligible phenomenological role [3,16]. Such scenarios are beyond the scope of the present work.

The simplifying assumptions (15) and (16) lead to a specific texture for the matrix U,

$$U \simeq \begin{pmatrix} U_{e1} & U_{e2} & 0 & 0 \\ U_{s1} & U_{s2} & U_{s3} & U_{s4} \\ 0 & 0 & U_{\mu 3} & U_{\mu 4} \\ U_{\tau 1} & U_{\tau 2} & U_{\tau 3} & U_{\tau 4} \end{pmatrix}, \tag{17}$$

[1]Although our work is focussed on 2+2 spectra, we will also briefly comment upon alternative 3+1 spectra (a triplet plus a loner state) in Sec. VII. In fact, the standard arguments against 3+1 models (see, e.g., [1]) appear now to be somewhat less compelling [12,19] in light of the most recent LSND data [6].

with the following implications. The state ν_μ (ν_e) must be a linear combination of ν_3 and ν_4 (ν_1 and ν_2),

$$\nu_\mu = +c_\psi \nu_3 + s_\psi \nu_4, \tag{18}$$

$$\nu_e = +c_\omega \nu_1 + s_\omega \nu_2, \tag{19}$$

where $c = \cos$, $s = \sin$, and we have introduced two mixing angles ψ and ω (ranging in $[0, \pi/2]$). The corresponding orthogonal combinations ν_+ and ν_-, defined as

$$\nu_+ = -s_\psi \nu_3 + c_\psi \nu_4, \tag{20}$$

$$\nu_- = -s_\omega \nu_1 + c_\omega \nu_2, \tag{21}$$

must be a linear combination of the remaining flavor states ν_τ and ν_s,

$$\nu_+ = +c_\xi \nu_\tau + s_\xi \nu_s, \tag{22}$$

$$\nu_- = -s_\xi \nu_\tau + c_\xi \nu_s, \tag{23}$$

where ξ is the third (and last) mixing angle needed to parametrize a unitary matrix U of the form (17). In terms of (ω, ψ, ξ), the matrix U reads explicitly

$$U = \begin{pmatrix} c_\omega & s_\omega & 0 & 0 \\ -s_\omega c_\xi & c_\omega c_\xi & -s_\psi s_\xi & c_\psi s_\xi \\ 0 & 0 & c_\psi & s_\psi \\ s_\omega s_\xi & -c_\omega s_\xi & -s_\psi c_\xi & c_\psi c_\xi \end{pmatrix}. \tag{24}$$

By defining the rotation matrices

$$U_\xi = \begin{pmatrix} 1 & 0 & 0 & 0 \\ 0 & c_\xi & 0 & s_\xi \\ 0 & 0 & 1 & 0 \\ 0 & -s_\xi & 0 & c_\xi \end{pmatrix}, \tag{25}$$

$$U_\psi = \begin{pmatrix} 1 & 0 & 0 & 0 \\ 0 & 1 & 0 & 0 \\ 0 & 0 & c_\psi & s_\psi \\ 0 & 0 & -s_\psi & c_\psi \end{pmatrix}, \tag{26}$$

and

$$U_\omega = \begin{pmatrix} c_\omega & s_\omega & 0 & 0 \\ -s_\omega & c_\omega & 0 & 0 \\ 0 & 0 & 1 & 0 \\ 0 & 0 & 0 & 1 \end{pmatrix}, \tag{27}$$

the mixing matrix U can also be written as

$$U = U_\xi U_{\psi\omega}, \tag{28}$$

where the commutation property $[U_\omega, U_\psi] = 0$ has been used:

$$U_{\psi\omega} \equiv U_\psi U_\omega = U_\omega U_\psi. \tag{29}$$

Finally, it is useful to introduce a new flavor basis ν'_α defined as

$$\nu'_\alpha = (\nu_e, \nu_-, \nu_\mu, \nu_+)^T, \tag{30}$$

related to the standard flavor basis by a ξ-rotation,

$$\nu'_\alpha = U_\xi^T \nu_\alpha . \tag{31}$$

In such basis, the neutrino evolution Hamiltonian reads

$$\mathcal{H}' = \frac{1}{2E} U_{\psi\omega} \mathcal{M} U_{\psi\omega}^T + \sqrt{2} G_F U_\xi^T \mathrm{diag}\left(N_e, \frac{1}{2} N_n, 0, 0 \right) U_\xi . \tag{32}$$

In the next subsection, it will be shown how the above 4ν Hamiltonian can be effectively decoupled in two (solar and atmospheric) 2ν sub-Hamiltonians.

Effective Hamiltonians for mixed active-sterile oscillations in matter have been recently discussed also in Refs. [3,16]. We can make contact with the ϕ_{ij} notation of [3] through the identifications $\omega = \phi_{12}$, $\psi = \phi_{34}$, and $\xi = \phi_{24}$, valid under the approximations $\phi_{23} \simeq 0$ [equivalent to Eq. (15)] and $\phi_{13} \simeq \phi_{14} \simeq 0$ [equivalent to Eq. (16)]. Analogously, we can make contact with the θ_{ij} notation of [16] through the identifications $\xi = \theta_{34}$ and $\psi = \theta_{24}$, valid under the approximation $\theta_{23} \simeq 0$ [equivalent to Eq. (15)].

C. Approximations related to atmospheric ν's

As far as atmospheric neutrinos are concerned, we neglect in first approximation the small (ν_1, ν_2) mass square difference δm^2, and take the inter-doublet mass square difference M^2 very large. The matrix $\mathcal{M}$ in Eq. (8) for atmospheric neutrinos can then be written as

$$\mathcal{M}_A \simeq \mathrm{diag}(-M^2, -M^2, 0, m^2). \tag{33}$$

By inserting such $\mathcal{M}_A$ in Eq. (32), one obtains that (i) The angle ω is rotated away; and (ii) as $M^2 \to \infty$, the states (ν_e, ν_-) [or, equivalently, (ν_1, ν_2)] oscillate with very high frequency $(\propto M^2)$, and effectively decouple from the states (ν_μ, ν_+). Therefore, only the evolution of (ν_μ, ν_+) is relevant,

$$i \frac{d}{dx} \begin{pmatrix} \nu_\mu \\ \nu_+ \end{pmatrix} \simeq \mathcal{H}'_A \begin{pmatrix} \nu_\mu \\ \nu_+ \end{pmatrix}, \tag{34}$$

the Hamiltonian being given by

$$\mathcal{H}'_A = \frac{m^2}{4E} \begin{pmatrix} c_{2\psi} & s_{2\psi} \\ s_{2\psi} & -c_{2\psi} \end{pmatrix} + \sqrt{2} G_F \begin{pmatrix} 0 & 0 \\ 0 & \frac{1}{2} s_\xi^2 N_n \end{pmatrix}, \tag{35}$$

where we have subtracted an inessential term $m^2/4E$ from the diagonal elements of $\mathcal{H}'_A$.

Equation (35) for atmospheric neutrinos is equivalent to the familiar one describing the $\nu_\mu \to \nu_s$ Hamiltonian, provided that the usual mass and mixing parameters are identified with m^2 and ψ, and that the neutron density N_n is multiplied by a factor s_ξ^2. For increasing values of s_ξ^2, one gets a smooth interpolation from pure $\nu_\mu \to \nu_\tau$ oscillations ($s_\xi^2 = 0$) to pure $\nu_\mu \to \nu_s$ oscillations ($s_\xi^2 = 1$), passing through mixed active-sterile transitions ($0 < s_\xi^2 < 1$).

Equation (35), which has been derived for the reference 4ν spectrum of Fig. 1, trivially holds also for for spectra with negative δm^2 or negative M^2 (being independent of such mass parameters). Concerning the case of negative m^2, one can easily prove (by swapping the states ν_3 and ν_4), that it is equivalent to the case of positive m^2, modulo the replacement $s_\psi \to c_\psi$ (and $\nu_+ \to -\nu_+$), which corresponds to swap the first two octants of ψ, and thus does not need a separate treatment (as far as $\psi \in [0, \pi/2]$). It follows that the sign of m^2 is irrelevant at the octant boundary ($\psi = \pi/4$), namely, at maximal atmospheric ν mixing. For atmospheric antineutrinos, the same considerations as for neutrinos apply, provided that the neutron density is taken with opposite sign.

D. Approximations related to solar ν's

As far as solar neutrinos are concerned, the atmospheric neutrino doublet (ν_3, ν_4) can be seen as a couple of ''far'' mass eigenstates, separated from (ν_1, ν_2) by a large M^2 gap. At zeroth order in $\delta m^2/m^2$ and in m^2/M^2, the matrix $\mathcal{M}$ in Eq. (8) for solar neutrinos can then be written as

$$\mathcal{M}_S \simeq \mathrm{diag}(0, \delta m^2, M^2, M^2). \tag{36}$$

By inserting such $\mathcal{M}_S$ in Eq. (32), one obtains that (i) The angle ψ is rotated away; and (ii) as $M^2 \to \infty$, the states (ν_μ, ν_+) [or, equivalently, (ν_3, ν_4)] oscillate with very high frequency $(\propto M^2)$, and effectively decouple from the states (ν_e, ν_-). Therefore, only the evolution of (ν_e, ν_-) is relevant,

$$i \frac{d}{dx} \begin{pmatrix} \nu_e \\ \nu_- \end{pmatrix} \simeq \mathcal{H}'_S \begin{pmatrix} \nu_e \\ \nu_- \end{pmatrix}, \tag{37}$$

the Hamiltonian being given by

$$\mathcal{H}'_S = \frac{\delta m^2}{4E} \begin{pmatrix} c_{2\omega} & s_{2\omega} \\ s_{2\omega} & -c_{2\omega} \end{pmatrix} + \sqrt{2} G_F \begin{pmatrix} N_e - \frac{1}{2} c_\xi^2 N_n & 0 \\ 0 & 0 \end{pmatrix}, \tag{38}$$

where we have subtracted an inessential term $(\delta m^2/4E + \sqrt{2} G_F \frac{1}{2} c_\xi^2 N_n)$ from the diagonal elements of $\mathcal{H}'_S$.

Equation (38) for solar neutrinos is equivalent to the familiar one describing two-family oscillations, provided that the usual mass and mixing parameters are identified with δm^2 and ω, and that the background fermion density is taken as $N_f = N_e - \frac{1}{2} c_\xi^2 N_n$. For increasing values of s_ξ^2, one gets a smooth interpolation between pure $\nu_e \to \nu_s$ oscillations ($s_\xi^2 = 0$ and $N_f = N_e - \frac{1}{2} N_n$) and pure $\nu_e \to \nu_\tau$ oscillations ($s_\xi^2 = 1$ and $N_f = N_e$), passing through mixed active-sterile transitions ($0 < s_\xi^2 < 1$).

Equation (38), which has been derived for the 4ν reference spectrum of Fig. 1, trivially holds also for spectra with

negative m^2 or negative M^2 (being independent of such mass parameters). Concerning the case of negative δm^2, one can easily prove (by swapping the states ν_1 and ν_2), that it is equivalent to the case of positive δm^2, modulo the replacement $s_\omega \to c_\omega$ (and $\nu_- \to -\nu_-$), which correspond to swap the first two octants of ω, and thus does not need a separate treatment (as far as $\omega \in [0,\pi/2]$). It follows that the sign of δm^2 is irrelevant at the octant boundary ($\omega = \pi/4$), namely, at maximal solar ν mixing.

E. Summary and remarks about the 4ν framework

We have introduced a 2+2 four-neutrino scenario, based on a few phenomenological approximations, which embeds at the same time both active and sterile oscillations of atmospheric and solar neutrinos. The final states ν_+ and ν_- for atmospheric and solar flavor transitions ($\nu_\mu \to \nu_+$ and $\nu_e \to \nu_-$, respectively) represent orthogonal combinations of ν_τ and ν_s through a mixing angle ξ [Eqs. (22) and (23)].

The angle ξ governs the relative amount of ν_s and ν_τ in the states $\nu_\pm$, and thus also the amplitude of matter effects. When $\xi \to 0$, the state ν_+ (oscillation partner of ν_μ) is dominantly a ν_τ, while the state ν_- (oscillation partner of ν_e) is dominantly a ν_s; and vice versa for $\xi \to \pi/2$. For $\xi = \pi/4$, both solar and atmospheric neutrino oscillations are simultaneously and democratically distributed into the active and sterile channels.

Atmospheric neutrino oscillations are governed by an effective 2ν Hamiltonian with vacuum mass-mixing parameters (m^2, ψ), and with an effective fermion density in matter given by $N_f = \frac{1}{2} s_\xi^2 N_n$ [Eq. (35)]. The case of negative m^2 is equivalent to swap the first two octants of ψ, and thus it does not need a separate treatment.

Solar neutrino oscillations are governed by an effective 2ν Hamiltonian with vacuum mass-mixing parameters $(\delta m^2, \omega)$, and with an effective fermion density in matter given by $N_f = N_e - \frac{1}{2} c_\xi^2 N_n$ [Eq. (38)]. The case of negative δm^2 is equivalent to swap the first two octants of ω, and thus it does not need a separate treatment.

The sign of M^2 (namely, the occurrence of a solar ν doublet heavier or lighter than the atmospheric ν doublet) is irrelevant under our approximations, as far as current oscillation experiments are concerned. Such a sign can instead be relevant in other contexts, such as in supernovae (see, e.g., [21]) in big-bang nucleosynthesis (BBN) (see, e.g., [22,23] and references therein) and, for Majorana neutrinos, in neutrinoless double beta decay ($0\nu2\beta$) (see, e.g., [24–26] and references therein). In particular, BBN data can probe new (sterile) neutrino species in addition to the three active neutrinos, and thus constrain 4ν scenarios. However, at present, such constraints do not appear to be stable enough [27] to really exclude specific 4ν models with great confidence, especially if one elaborates upon a possible tension between the most recent BBN and cosmic microwave background data [28]. Moreover, subtle effects of sterile neutrino oscillations in the early universe [29], which are still subject to intensive studies (see [30] and references therein) might provide ways to evade or mitigate standard BBN bounds. Constraints from $0\nu2\beta$ decay can also be evaded by assuming Dirac neutrinos. For such reasons, we postpone the discussion of (potentially important but presently uncertain) additional BBN and $0\nu2\beta$ bounds to a future work, while in this paper we prefer to focus on a homogeneous set of neutrino oscillation data (SK atmospheric).

Finally, we point out that the reduction from the general 4ν oscillation Hamiltonian (32) to effective 2ν forms for both atmospheric and solar neutrinos [Eqs. (35) and (38), respectively] justifies *a posteriori* our neglect of CP violation phases (unobservable in 2ν scenarios), and thus the initial position (14). An alternative proof of the vanishing of (observable) CP violation effects in our framework can also be obtained by applying our approximations (13), (15) and (16) to the 4ν Jarlskog invariants explictly worked out in [31].

III. GRAPHICAL REPRESENTATIONS

In our 4ν framework, it turns out that the mixing parameter spaces for atmospheric and solar neutrinos can be usefully represented in triangular plots, embedding unitarity relations of the kind $U_1^2 + U_2^2 + U_3^2 = 1$ through the heights projected within a triangle with equal sides (and unit total height).[2] Such unitarity relations hold for the four columns of the mixing matrix U characterizing our framework [Eq. (17)], and can be separated into two constraints on the atmospheric (ν_3, ν_4) doublet,

$$U_{\mu 3}^2 + U_{\tau 3}^2 + U_{s3}^2 = 1, \tag{39}$$

$$U_{\mu 4}^2 + U_{\tau 4}^2 + U_{s4}^2 = 1, \tag{40}$$

and two constraints on the solar (ν_1, ν_2) doublet,

$$U_{e1}^2 + U_{\tau 1}^2 + U_{s1}^2 = 1, \tag{41}$$

$$U_{e2}^2 + U_{\tau 2}^2 + U_{s2}^2 = 1. \tag{42}$$

As we will see below, it is sufficient to implement just one unitarity relation in one triangle plot for each doublet, the other relation being a consequence. We choose to implement Eq. (40) for atmospheric neutrinos and Eq. (42) for solar neutrinos.

Figure 2 represents the ''atmospheric neutrino triangle,'' embedding the unitarity constraint (40), which is related to the flavor composition of ν_4,

$$\nu_4 = U_{\mu 4}\nu_\mu + U_{\tau 4}\nu_\tau + U_{s4}\nu_s \tag{43}$$

$$= s_\psi \nu_\mu + c_\psi c_\xi \nu_\tau + c_\psi s_\xi \nu_s \tag{44}$$

$$= s_\psi \nu_\mu + c_\psi \nu_+ . \tag{45}$$

In the triangle plot, the upper, lower left and lower right corner are identified with ν_μ, ν_τ, and ν_s, respectively. The heights projected from a generic point ν_4 inside the triangle

[2]Triangle plots have been already introduced and discussed in detail in the context of 3ν mixing, see [32,33].

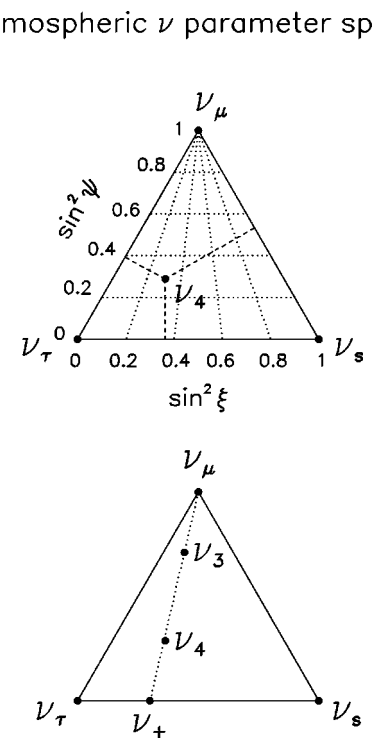

FIG. 2. The atmospheric ν parameter space, in the triangular representation. See the text for details.

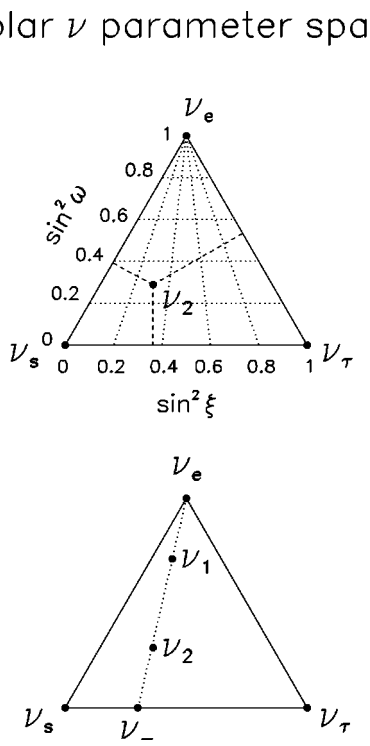

FIG. 3. The solar ν parameter space, in the triangular representation. See the text for details.

onto the lower, right, and left side represent the elements $U^2_{\mu 4}$, $U^2_{\tau 4}$, and U^2_{s4}, respectively. When ν_4 coincides with one of the corners (mass eigenstate = flavor eigenstate), no oscillation occurs. Generic inner points describe mixed (active+sterile) atmospheric neutrino oscillations, smoothly interpolating from pure $\nu_\mu \to \nu_\tau$ (left side) to pure $\nu_\mu \to \nu_s$ (right side). In the upper triangle plot of Fig. 2, the (s^2_ψ, s^2_ξ) parametrization is also charted. The lower triangle plot shows explicitly that ν_4 is a linear combination of ν_μ and ν_+, with ν_+ confined to the lower side (being a linear combination of ν_τ and ν_s). Notice that, once the point $\nu_4 = (s^2_\xi, s^2_\psi)$ is fixed, the position of ν_3 is also determined in the same plot at the coordinates (s^2_ξ, c^2_ψ), and there is no need for a separate triangle embedding the constraint (39). The points ν_3 and ν_4 are then symmetrically placed onto the line joining the states ν_μ and ν_+ (of which they are orthogonal combinations).

Figure 3 represents the ''solar neutrino triangle,'' embedding the unitarity constraint (42), which is related to the flavor composition of ν_2,

$$\nu_2 = U_{e2}\nu_e + U_{\tau 2}\nu_\tau + U_{s2}\nu_s \tag{46}$$

$$= s_\omega \nu_e - c_\omega s_\xi \nu_\tau + c_\omega s_\xi \nu_s \tag{47}$$

$$= s_\omega \nu_e + c_\omega \nu_- . \tag{48}$$

In the triangle plot, the upper, lower left and lower right corner are identified with ν_e, ν_s, and ν_τ, respectively. The heights projected from a generic point ν_2 inside the triangle onto the lower, right, and left side represent the elements U^2_{e2}, U^2_{s4}, and $U^2_{\tau 4}$, respectively. When ν_2 coincides with one of the corners (mass eigenstate = flavor eigenstate), no oscillation occur. Generic inner points describe mixed (active+sterile) solar neutrino oscillations, smoothly interpolating from pure $\nu_\mu \to s$ (left side) to pure $\nu_\mu \to \nu_\tau$ (right side). In the upper triangle plot of Fig. 3, the (s^2_ψ, s^2_ω) parametrization is also charted. The lower triangle plot shows explicitly that ν_2 is a linear combination of ν_e and ν_-, with ν_- confined to the lower side (being a linear combination of ν_s and ν_τ). Notice that, once the point $\nu_2 = (s^2_\xi, s^2_\omega)$ is fixed, the position of ν_1 is also determined in the same plot with coordinates (s^2_ξ, c^2_ω), and there is no need for a separate triangle embedding the constraint (41). The points ν_1 and ν_2 are then symmetrically placed onto the line joining the states ν_e and ν_- (of which they are orthogonal combinations).

Finally, Fig. 4 shows the link between the solar and atmospheric parameter spaces, which follows from the fact that the variable $\sin^2\xi$ must represent the same abscissa in both triangles of Figs. 2 and 3. By putting the two triangles on top of each other, it follows that the ν_+ and ν_- points must be placed on the same vertical line, and that couple of points inside the atmospheric and solar triangles must be placed on iso-s^2_ξ lines (slanted dashed lines in Fig. 4). It will be shown that such ''common ξ'' constraint will significantly reduce the solutions that would be separately allowed by solar data only or by atmospheric data only.

IV. SUPER-KAMIOKANDE ATMOSPHERIC ν DATA AND EXPECTATIONS

In the previous sections we have set the theoretical framework, as well as the graphical representations, for our analy-

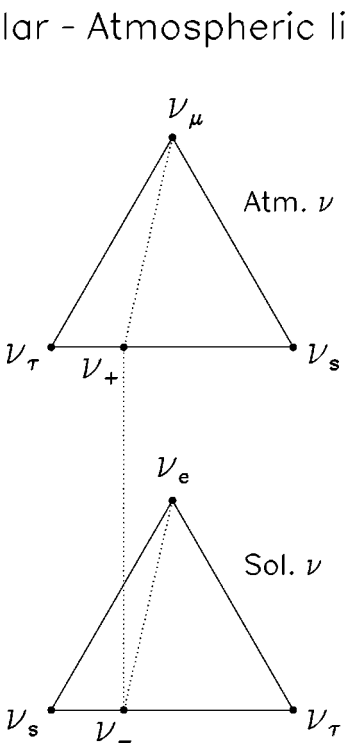

FIG. 4. Graphical representation of the link existing between the solar and atmospheric parameter spaces.

sis of 4ν oscillation solutions to the atmospheric ν anomaly. In this section we present the data used in the fit, and make a first discussion (to be refined later) of the relative importance of different data samples in constraining the mixing of atmospheric ν_μ with ν_s.

Figure 5 shows the Super-Kamiokande data used in our χ^2 analysis, as graphically reduced from [7], corresponding to a detector exposure of 70.5 kTy. The reported errors are statistical only ($\pm 1\sigma$). Systematic errors are treated as in [32]. The data are shown as binned distributions of *e*-like and μ-like event rates *R*, normalized to no-oscillation expectations R_0 in each bin, in terms of the lepton zenith angle ϑ. The distributions refer to sub-GeV (SG) leptons, multi-GeV (MG) leptons, upward stopping (US) muons, and upward through-going (UT) muons, according to the SK terminology

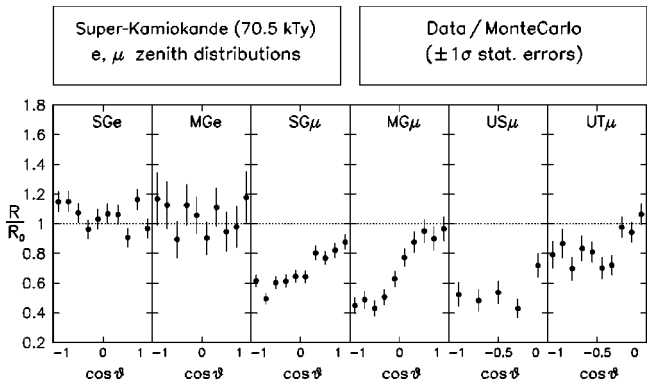

FIG. 5. Super-Kamiokande data on the zenith distributions of lepton events induced by atmospheric neutrinos.

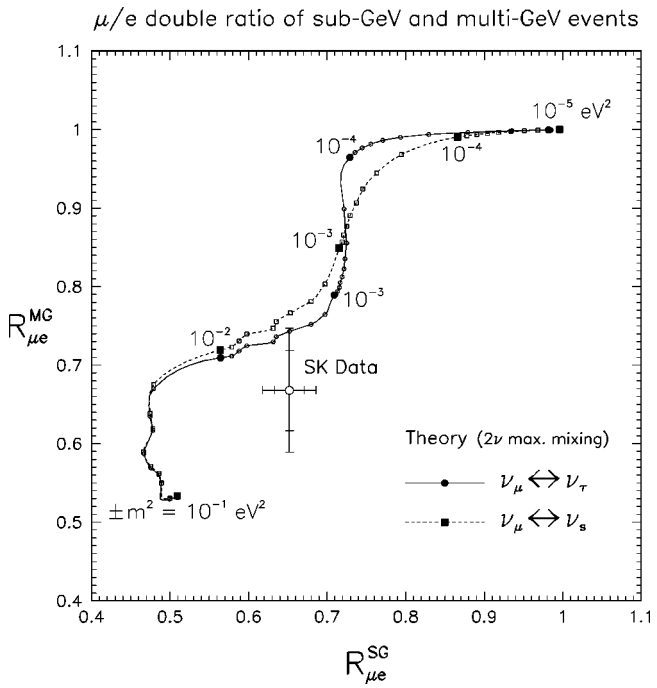

FIG. 6. Double ratio of muon-to-electron events for multi-GeV events (*y*-axis) and sub-GeV events (*x*-axis). The theoretical expectation at fixed (maximal) mixing and for running m^2 is shown as a solid curve for pure active oscillations, and as a dashed curve for pure sterile oscillations. The cross with error bars (statistical and total) represents the SK data.

[7,32]. The total number of data points used in the fit is 55. The SK data on neutral-current enriched samples [8], which are also useful in testing the presence of a ν_s component [34], are not included in the present analysis.

Although our main results are based on accurate calculations [32] of the full zenith distributions in Fig. 5, it is useful to gain some prior understanding of the physics by means of (partly) averaged quantities such as the popular μ/e double flavor ratio for SG and MG events, the up-down asymmetry of MG events, and the vertical-to-horizontal ratio of UT events. We follow the SK conventions for such quantities [7,8], namely, data with $|\cos\vartheta|<0.2$ are removed in the up-down asymmetry, and the separation between ''vertical'' and ''horizontal'' through-going muons is conventionally taken at $\cos\vartheta=-0.4$.

Figure 6 shows the double ratio $R_{\mu/e}$ of MG events vs SG events. The corresponding SK data are shown as a cross (with statistical and total 1σ error bars). The theoretical expectations at maximal mixing are shown as a solid line for pure $\nu_\mu \to \nu_\tau$ oscillations ($s^2_\xi=0$ in our notation) and as a dashed line for pure $\nu_\mu \to \nu_s$ oscillations ($s^2_\xi=1$). Such lines connect the points calculated at $\pm m^2 = n\times 10^m$ eV^2, with $m=-5,-4,\ldots,-1$, and $n=1,2,\ldots,9$ (the sign of m^2 is irrelevant at maximal mixing, $s^2_\psi=1/2$). Cases with $0<s^2_\xi<1$ (not shown) would give lines intermediate between the solid and the dashed ones. The ''trajectories'' of the theoretical points start at $R_{\mu/e}\simeq 1$ for small m^2 (no-oscillation limit), and end at $R_{\mu/e}\simeq 1/2$ for large m^2 (averaged oscillations).

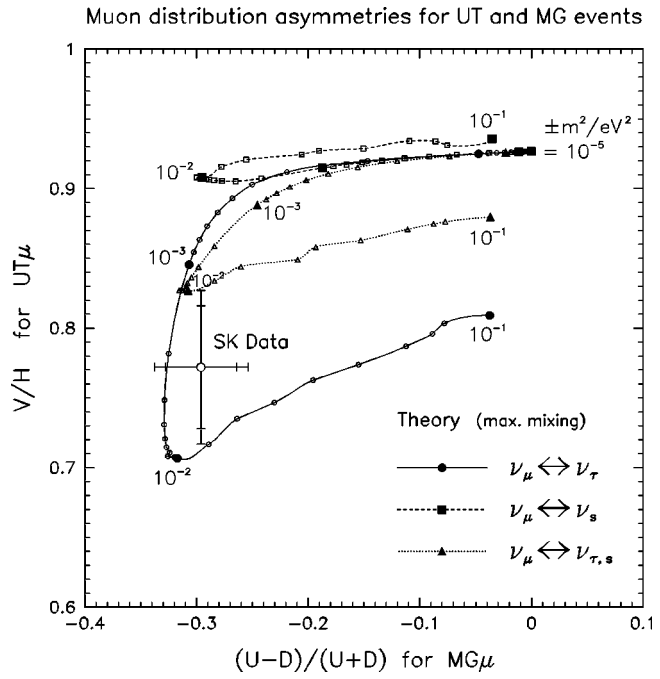

FIG. 7. Vertical-to-horizontal ratio of upgoing muon rates *vs* the up-down asymmetry of multi-GeV muon events. The theoretical expectation at fixed (maximal) mixing and for running m^2 is shown as a solid curve for pure active oscillations, as a dashed curve for pure sterile oscillations, and as a dotted curve for mixed active +sterile oscillations of equal amplitude. The cross with error bars represents the SK data.

From Fig. 6 we learn that the double ratio is not a good variable to discriminate between $\nu_\mu \to \nu_\tau$ and $\nu_\mu \to \nu_s$ oscillations, since the separation of the two corresponding curves is much smaller than the experimental error. In fact, the matter effects which should distinguish the ν_s channel are suppressed both by the relatively low energy of SG and MG events and by integration over the zenith angle. On the other hand, the combined SG and MG information on $R_{\mu/e}$ in Fig. 6 is sensitive to m^2, and favors the range $\sim[10^{-3},10^{-2}]$ eV^2, with $\sim 4\times10^{-3}$ eV^2 being the value closest to the data for both oscillation channels. We conclude that the SG and MG μ/e double ratios give valuable information on m^2, rather than on the flavor of the ν_μ oscillation partner.

A better sensitivity to the sterile component of the ν_μ oscillation partner can be gained by improving the zenith angle information and by probing higher energies, where matter effects are larger [35]. Figure 7 shows the ratio of vertical to horizontal (V/H) upward through-going muons vs the up-down asymmetry of multi-GeV muons ($U-D/U+D$). As in Fig. 6, solid (dashed) lines refer to $\nu_\mu \to \nu_\tau$ ($\nu_\mu \to \nu_s$) oscillations at maximal mixing, $s^2_\psi = 1/2$. In addition, Fig. 7 shows, as a dotted line, the case of mixed active-sterile oscillations with equal amplitude [$\nu_+ = (\nu_s + \nu_\tau)/\sqrt{2}$, namely, $s^2_\xi = 1/2$]. The trajectories of the theoretical points start and end at small values of the up-down asymmetry, as expected in the limits $m^2 \to 0$ (no oscillation) and $m^2 \to \infty$ (averaged oscillations), after passing through negative values (corresponding to a suppression of the upgoing muon rate). The V/H ratio should also take back its no-oscillation value as $m^2 \to \infty$, although the highest values reported in Fig. 7 ($m^2 = 10^{-1}$ eV^2) is not ''asymptotic'' enough to show this behavior. The V/H variations with m^2 are rather small in the pure $\nu_\mu \to \nu_s$ case, when compared with the corresponding variations in the pure $\nu_\mu \to \nu_\tau$ case, as a consequence of the strong damping of the sterile transition amplitude in matter at high energies [35]. Intermediate variations of V/H occur for the mixed active+sterile case (dotted line); therefore, the V/H asymmetry is a sensitive probe of s^2_ξ through the effects of the matter term $\sqrt{2} G_F s^2_\xi N_n/2$.

The recent SK data [7], shown in Fig. 7 as a cross with error bars (statistical and total at 1σ) clearly favor the pure $\nu_\mu \to \nu_\tau$ case (solid line), as compared with the pure $\nu_\mu \to \nu_s$ case (dashed line). By themselves, such data cannot exclude an intermediate situation with large mixing of ν_μ with ν_τ *and* ν_s (dotted line). In such case, however, the favored values of m^2 are rather large [$\sim O(10^{-2}]$ eV^2), in contrast with the information coming from the μ/e ratio in Fig. 6. Therefore, the interplay of different pieces of data seems to indicate clearly an upper bound on the ν_s component of ν_+ (namely, on s^2_ξ).

V. RESULTS OF THE ATMOSPHERIC ν ANALYSIS

In this section we present the results of our fit to the atmospheric neutrino data of Fig. 5 (55 data points), as obtained by calculating the SK zenith distributions for unconstrained values of the three relevant parameters (m^2, s^2_ξ, s^2_ψ). We discuss first the bounds on the mass parameter m^2, and then those on the mixing parameters (s^2_ξ, s^2_ψ).

Figure 8 shows the value of the global χ^2 as a function of m^2 (in linear scale), for four $\nu_\mu \to \nu_+$ oscillation cases, corresponding to: (i) unconstrained ν_+ (thick solid line); (ii) $\nu_+ = \nu_\tau$ (thin solid line); (iii) $\nu_+ = \nu_s$ (dashed line); and (iv) $\nu_+ = (\nu_s + \nu_\tau)/\sqrt{2}$ (dotted line). In terms of the mixing angle ξ, such cases correspond, respectively, to (i) unconstrained s^2_ξ; (ii) $s^2_\xi = 0$; (iii) $s^2_\xi = 1$; and (iv) $s^2_\xi = 1/2$. The parameter s^2_ψ is left free in all four cases. The global minimum for the unconstrained case ($\chi^2_{\rm min} = 47.4$) is reached at $(m^2/\text{eV}^2, s^2_\xi, s^2_\psi) = (3.2\times10^{-3}, 0.18, 0.51)$. The slight preference for a nonzero value of s^2_ξ at the point of minimum χ^2 is intriguing, but not statistically significant, since the fit with $s^2_\xi = 0$ (pure $\nu_\mu \to \nu_\tau$ oscillations, thin solid line) is only slightly worse than the unconstrained fit (thick solid line).

Concerning the statistical interpretation of the results shown in Fig. 8, some remarks are in order. In general, one can use the χ^2 function for two complementary purposes [36]: (1) to estimate the best-fit values of (m^2, s^2_ξ, s^2_ψ) and their uncertainties (*parameter estimation*); or (2) to test the goodness-of-fit with some prior assumptions about (m^2, s^2_ξ, s^2_ψ) (*hypothesis test*). In the first approach, the values of (m^2, s^2_ξ, s^2_ψ) minimizing the χ^2 function are taken as best estimates of the (unknown) true values of such parameters. The corresponding uncertainties are then obtained by allowing a shift in the χ^2 function ($\Delta\chi^2 = \chi^2 - \chi^2_{\rm min}$), with corresponding confidence levels determined by the number of free

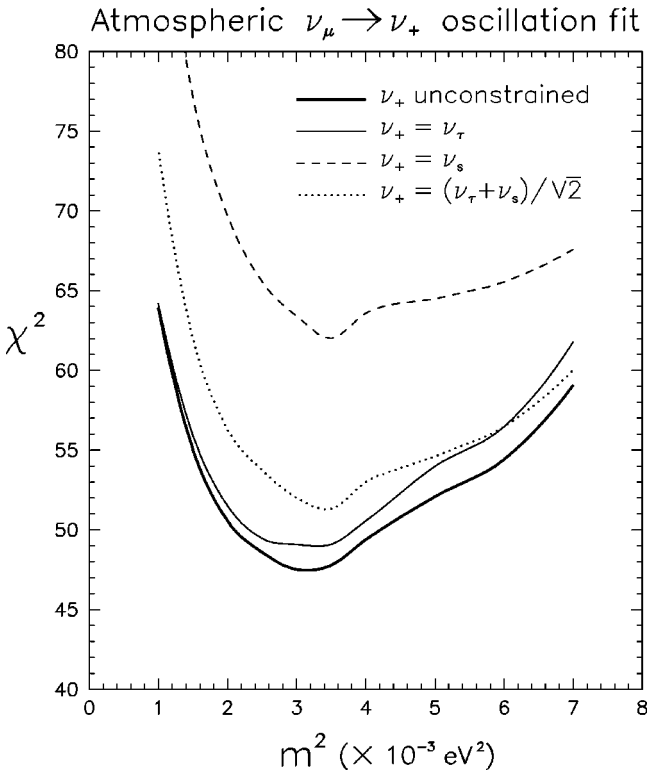

FIG. 8. Result of the global χ^2 fit to the 55 data points of Fig. 5, as a function of the mass parameter m^2, assuming $\nu_\mu \to \nu_+$ oscillations for atmospheric neutrinos, and different options for ν_+. The mixing angle s^2_ψ is left unconstrained in all cases. The case $\nu_+ = \nu_s$ provides the worst fit, but one cannot exclude a sizable ν_s component of ν_+.

parameters in the model ($N_{\rm DF}=3$ in our case). From this point of view, the case of pure $\nu_\mu \to \nu_s$ oscillations, corresponding to $\Delta\chi^2/N_{\rm DF}=14.7/3$ in Fig. 8, is reached only at 99.8% C.L., and is thus strongly disfavored. In the second approach, one checks how well a specific hypothesis about the parameters fits the 55 SK data points, independently of the existence of a global χ^2 minimum at some point in the parameter space. For instance, if order to test the *a priori* hypotheses of pure $\nu_\mu \to \nu_\tau$ or pure $\nu_\mu \to \nu_s$ oscillations, one should compare the absolute χ^2 value with $N_{\rm DF}=55-2$, the two free variables being m^2 and s^2_ψ (s^2_ξ being fixed at 0 or 1, respectively). From Fig. 8, we then get that the probability of having a worse χ^2 is 63% for $s^2_\xi=0$ (pure $\nu_\mu \to \nu_\tau$ oscillations, $\chi^2/N_{\rm DF}=49/53$) and 18% for $s^2_\xi=1$ (pure $\nu_\mu \to \nu_s$ oscillations, $\chi^2/N_{\rm DF}=62/53$). Therefore, although the pure sterile case is clearly disfavored *in comparison* with the pure active case, it is not ruled out *a priori* in our oscillation analysis. Having clarified such statistical issues, we proceed to estimate the mass-mixing parameters (m^2, s^2_ξ, s^2_ψ) by using the first approach, based on $\Delta\chi^2$.

In Fig. 8, all four cases show a preference for $m^2 \simeq 3 \times 10^{-3}$ eV^2, which thus represents a very stable indication coming from the SK data, independently of the amplitude of the ν_s component. For the most general case (unconstrained ν_+) we obtain

$$m^2 \simeq 3.2^{+2.3}_{-1.6} \times 10^{-3} \ \text{eV}^2 (90\%\ \text{C.L.}), \tag{49}$$

by taking $\Delta\chi^2=6.25$ for $N_{\rm DF}=3$.

Figure 8 also gives gives indications about the parameter s^2_ξ. The case $s^2_\xi=0$ (thin solid line) gives results comparable to the best fit for unconstrained s^2_ξ (thick solid line). The case of a fifty-fifty admixture of ν_s and ν_τ in ν_+ ($s^2_\xi=1/2$, dotted line) provides a fit that, although worse than for pure $\nu_\mu \to \nu_\tau$, is still acceptable (its minimum χ^2 being only four units above the absolute minimum). However, the quality of the fit worsen rapidly as ν_+ gets closer to ν_s, the worst case being reached for pure $\nu_\mu \to \nu_s$ oscillations (dashed line). Therefore, we expect to get an upper bound on s^2_ξ from the analysis of the mixing parameters, which can be clearly represented in the triangle plot.

Figures 9 and 10 show the results of our analysis in the atmospheric triangle plot, for 10 representative (decreasing) values of m^2. The first three columns of triangles refer to the separate fits to sub-GeV electrons and muons (10+10 bins), multi-GeV electrons and muons (10+10 bins), and upward stopping and through-going muons (5+10 bins), while the fourth column refers to the total SK data sample (55 bins). For each column, we find the minimum χ^2 from the fit to the corresponding data sample, and then present sections of the allowed volume at fixed values of m^2 for $\Delta\chi^2=6.25$ (90% C.L., solid lines) and $\Delta\chi^2=11.36$ (99% C.L., dotted lines). It can be seen that the low-energy SG data are basically insensitive to s^2_ξ, since they are consistent both with $\nu_\mu \to \nu_\tau$ oscillations (left side) and with $\nu_\mu \to \nu_s$ oscillations (right side), as well as with any intermediate combination of the two oscillation channels. High-energy upgoing μ data are instead much more sensitive to the ν_s component through matter effects, which increase both with energy and with s^2_ξ, and tend to suppress the μ deficit [35]. Large matter effects appear to be disfavored by the upgoing muon data, the rightmost part of the triangle being excluded at 90% C.L. The multi-GeV data cover an intermediate energy range and are not as constraining as the upgoing muons; however, they also show a tendency to disfavor a large ν_s component. This tendency is strengthened in the global combination of data (fourth column), leading to the upper bound

$$s^2_\xi \lesssim 0.67 (90\%\ \text{C.L.}), \tag{50}$$

which clearly disfavors pure or quasi-pure $\nu_\mu \to \nu_s$ oscillations. In particular, from our Figs. 9 and 10 we derive that pure $\nu_\mu \to \nu_s$ oscillations ($s^2_\xi=1$) are excluded at $>99\%$ C.L., consistently with the SK analysis [7,8].

However, the bound (50) still allows intermediate cases of combined active+sterile oscillations with a sizable ν_s component. For instance, one cannot exclude that the sterile neutrino channel may have the same amplitude as the active one ($s^2_\xi=0.5$), or may even be dominant (e.g., $s^2_\xi=0.6$, corresponding to $\nu_+ \simeq 0.77\nu_s + 0.65\nu_\tau$). Furthermore, for m^2 in its upper range (e.g., $m^2=5\times10^{-3}$ eV^2 in Fig. 9), a subdominant ν_s component actually helps in the global fit to SK data,

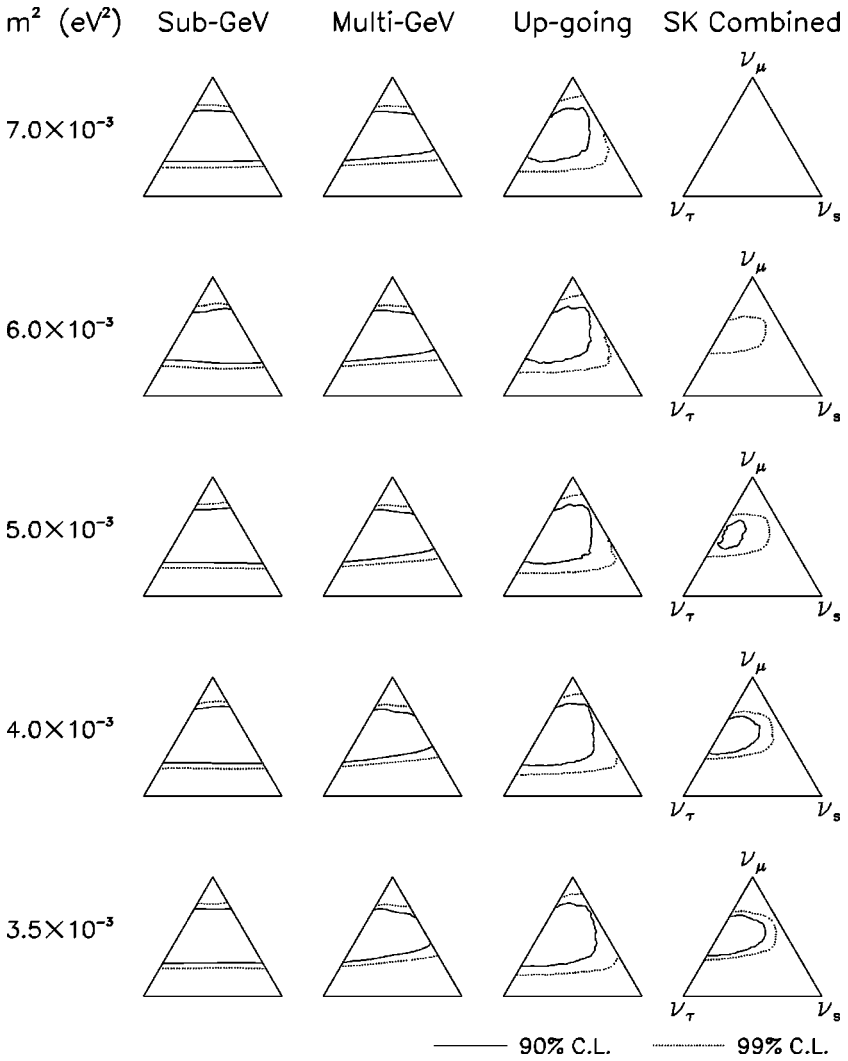

FIG. 9. Results of the global χ^2 fit to atmospheric neutrino data in the triangular representation, for decreasing values of m^2. See the text for details.

leading to a 90% C.L. allowed region which does not touch the left side of the triangle (corresponding to the pure $\nu_\mu \to \nu_\tau$ channel).

Figures 9 and 10 also provide bounds on the other mixing parameter s^2_ψ, which governs the relative amount of ν_μ and ν_+ on the atmospheric neutrino states ν_3 and ν_4 [see Eqs. (18),(20) and Fig. 2], and thus the overall amplitude of $\nu_\mu \to \nu_+$ oscillations. From Figs. 9 and 10 we derive

$$s^2_\psi \simeq 0.51 \pm 0.17 (90\%\ \text{C.L.}), \tag{51}$$

which favors $\nu_\mu \to \nu_+$ oscillations with nearly maximal amplitude, as one expects from the observation of nearly maximal average suppression ($\sim 50\%$) of upgoing MG muons. There is a slight asymmetry of the allowed regions with respect to $s^2_\psi = 1/2$, which reflects the relative change of sign of vacuum and matter terms in Eq. (35) when passing from the first to the second octant.

Figures 8, 9, and 10 demonstrate that, on the basis of present SK data on the zenith distributions of leptons induced by atmospheric neutrinos, pure $\nu_\mu \to \nu_s$ oscillations are strongly disfavored, but one cannot exclude mixed active-sterile $\nu_\mu \to \nu_+$ oscillations with $\nu_+ = c_\xi \nu_\tau + s_\xi \nu_s$, provided that the partial amplitude of the sterile channel is $\lesssim 67\%$ [Eq. (50)]. Since such bound is dominated by high-energy muons, it is important to understand how such data can improve the sensitivity to s^2_ξ in the future.

Figure 11 shows the zenith distributions of upward through-going muons at maximal (ν_μ, ν_+) mixing ($s^2_\psi = 1/2$) for $\nu_+ = \nu_\tau$ (left panel), $\nu_+ = (\nu_\tau + \nu_s)/\sqrt{2}$ (middle panel), and $\nu_+ = \nu_s$ (right panel). The solid (dashed) histograms refer to $\pm m^2 = 3 \times 10^{-3}$ eV^2 (5×10^{-3} eV^2), the sign of m^2 being irrelevant at maximal mixing. From left to right, s^2_ξ increases and matter effects also grow with it, producing an increasing modulation of the zenith distributions. The modulation, which is very strong for the oscillation probability at fixed energies (not shown), is largely smeared out in Fig. 11 by integration over the energy spectrum and, to a lesser extent, by the presence of both ν and $\overline{\nu}$ (with opposite matter terms) in the atmospheric neutrino flux. Therefore, the modulation pattern of the UTμ distribution might be more clearly observed in future atmospheric ν experiments [37] aiming at improved energy reconstruction and μ^+/μ^- separation. Concerning the present SK data (Fig. 11), the large scatter of central values and the still large error bars prevent a clear discrimination of the theoretical distributions in the

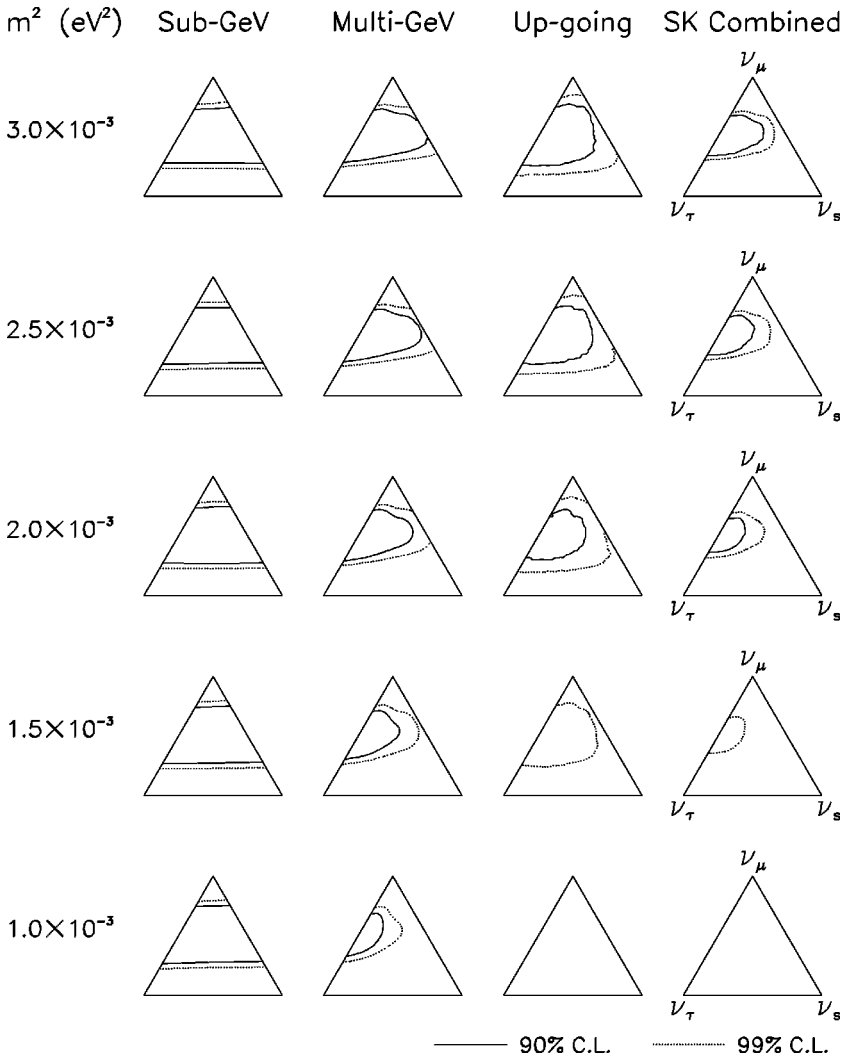

FIG. 10. As in Fig. 9, but for lower values of m^2.

left and middle panels, which anyway appear to provide a better fit than in the right panel. A reduction by a factor $\lesssim 2$ in the uncertainties of the SK UTμ sample appears necessary for a decisive discrimination among the three cases shown in Fig. 11. In conclusion, we can still learn a lot on the ν_s component of ν_+ as we get more high-energy muon data in SK, as well as in MACRO, and possibly from future atmospheric ν experiments.

VI. LINKING ATMOSPHERIC AND SOLAR NEUTRINOS

Solar neutrino oscillations with both active and sterile states have been recently investigated in [13,14], whose results can be interpreted, in our framework, through the identification $c_{23}^2 c_{24}^2 \equiv 1 - s_\xi^2$, $\theta_{12} = \omega$, and $\Delta m_{21}^2 = \delta m^2$. In [13,14] it has been shown that there is a continuous set of solutions to the solar neutrino problem for unconstrained s_ξ^2, ranging from pure ''active oscillation solutions'' ($s_\xi^2 = 1$) to pure ''sterile oscillation solutions'' ($s_\xi^2 = 0$). In particular, for $s_\xi^2 = 1$ all the usual solutions to the solar neutrino problem are present, either at small ω mixing (matter-enhanced solution) or at large ω mixing (matter-enhanced solution at low or high δm^2, or vacuum solutions). For decreasing values of s_ξ^2, all the solutions tend to shrink; however, the large mixing (LM) ones (vacuum or matter-enhanced) eventually disappear for $s_\xi^2 \lesssim 0.3-0.4$, while the small mixing (SM) solution still survives (at $\sim 99\%$ C.L.) even for $s_\xi^2 = 0$. Such behavior is qualitatively reported in Fig. 12, through the triangular representation of the parameter space. The plot is only qualitative, since the detailed behavior of any solution depends both on the confidence level adopted and on the specific value chosen for δm^2, whose complete scan is beyond the scope of this paper.

In Fig. 12, the allowed region at large mixing (s_ω^2 close to 1/2), which has the maximum likelihood at $s_\xi^2 = 1$ (pure active oscillations, right side of the triangle), gradually shrinks when s_ξ^2 decreases and eventually disappears. The allowed region at small mixing (s_ω^2 close to 0) covers instead the whole s_ξ^2 range.

As discussed in Secs. II and III, the solar and atmospheric solutions are coupled through the common angle ξ. Such coupling can be visualized by putting the solar and atmospheric triangles on top of each other, as shown in Fig. 4. The results are qualitatively different for the SM and LM solutions to the solar neutrino problem, as shown in Figs. 13 and 14.

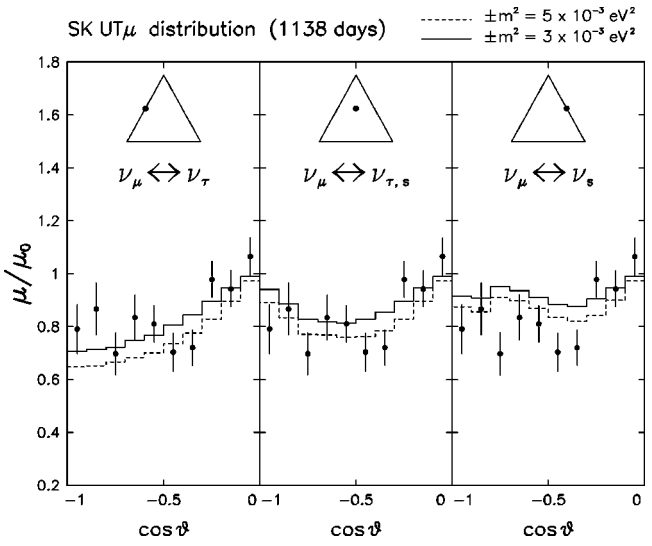

FIG. 11. The zenith distribution of upward through-going muon events for three different oscillation scenarios, involving pure active oscillations (left panel), pure sterile oscillations (right panel) and mixed active+sterile oscillations (middle panel) at maximal mixing.

Figure 13 shows, in gray, the regions globally allowed by the combination of solar and atmospheric ν data, assuming the SM solution to the solar ν problem. The fact that atmospheric ν data put an upper bound on s^2_ξ (as quantitatively discussed through Figs. 9 and 10) implies that also the fraction of the SM solar ν solution at large s^2_ξ is excluded. However, there is still a continuous range of global solutions for $s^2_\xi \neq 0$, having a sizable ν_s component for both solar and atmospheric ν oscillations. Therefore atmospheric ν data ''cut'' a fraction of the SM solution to the solar ν problem, but the combination still allows solutions involving active +sterile neutrino oscillations for both atmospheric and solar neutrinos.

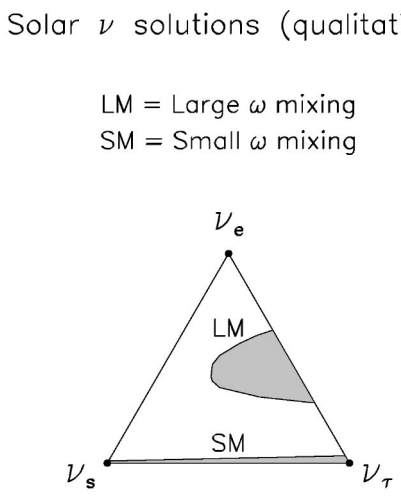

FIG. 12. Qualitative pattern of 4ν oscillation solutions to the solar neutrino problem at small or large mixing, in the triangular representation of the parameter space.

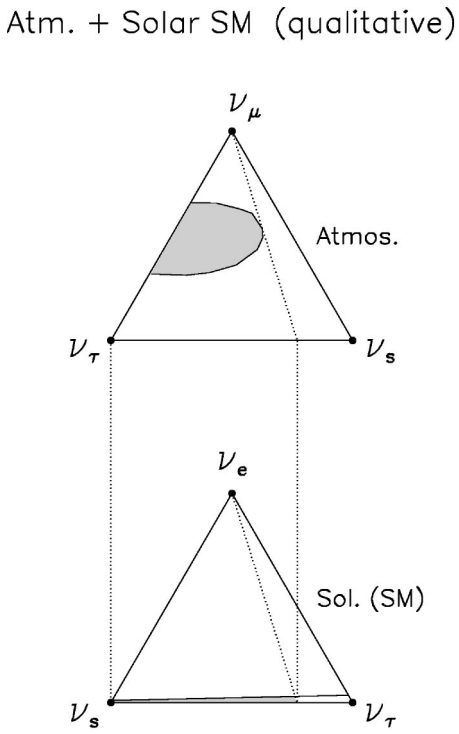

FIG. 13. Qualitative combination of the atmospheric ν solution with a typical small-angle solar ν solution.

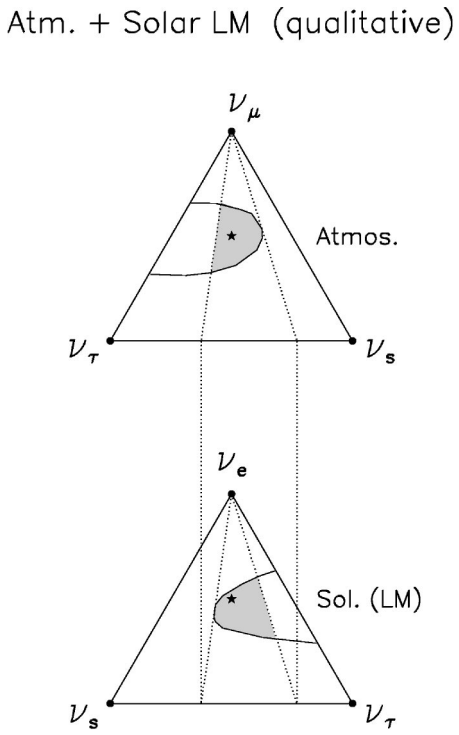

FIG. 14. Qualitative combination of the atmospheric ν solution with a typical large-angle solar ν solution.

The opposite happens for the LM solution to the solar neutrino problem. In this case, solar neutrino data cut the ''small s^2_ξ'' part of the atmospheric allowed region, as shown in Fig. 14, and the globally allowed solutions (gray inner regions) represent genuine active+sterile oscillations, which never reduce to the pure active or pure sterile subcases (the sides of the triangles). In particular, the points denoted by stars in Fig. 14 represent a peculiar solution (which might be dubbed ''fourfold maximal mixing''), corresponding to maximal mixing of $\nu_\pm$ with $\nu_{s,\tau}$ ($s^2_\xi = 1/2$), maximal mixing of $\nu_{3,4}$ with $\nu_{\mu,+}$ ($s^2_\psi = 1/2$), and maximal mixing of $\nu_{1,2}$ with $\nu_{e,-}$ ($s^2_\omega = 1/2$). In this case, both solar and atmospheric neutrino oscillations are equally distributed among the active and sterile channels.

In conclusion, it turns out that, at least qualitatively, 4ν scenarios with mixed active+sterile transitions for both solar and atmospheric neutrinos are allowed by the combination of world oscillation data, with different mixing patterns dictated by the solution assumed for the solar neutrino problem (either small or large mixing). Consistency between atmospheric and solar neutrino data in 4ν models has also been recently found in an independent and somewhat different analysis [16]. Therefore, the hypothesis of a fourth, sterile neutrino is still compatible with present data and needs further theoretical and experimental investigations. Such results clearly demonstrate that the two-flavor approximations often used to analyze solar or atmospheric neutrinos data (in terms of either pure active or pure sterile oscillations) are, in general, not appropriate to explore the full parameter space allowed by 4ν models. Our 4ν formalism and triangular representations can also be usefully applied to explore the $\nu_\mu \to \nu_s$ discovery potential in long baseline accelerator experiments, as shown for the MINOS experiment in [38].

VII. REMARKS ON 3+1 MASS SPECTRA

The standard arguments disfavoring 3+1 spectra (triplet +singlet) with respect to 2+2 spectra (two doublets) in the interpretation of the current 4ν oscillation phenomenology [1] appear to be somewhat weakened [12,19] in light of the most recent LSND data [6], and should be perhaps revisited quantitatively. Here we make just a few qualitative comments on the mixing pattern that is likely to emerge in 3+1 models characterized by a triplet (ν_1, ν_2, ν_3) (mainly responsible for solar and atmospheric oscillations) and by a ''loner'' state ν_4 (mainly responsible for LSND oscillations).

The absence (or weak occurrence, as in LSND) of oscillations in all channels probed by short-baseline reactor and accelerator experiments is consistent with ν_4 being close to a flavor eigenstate. The dominant flavor of ν_4 cannot be ν_e (ν_μ), otherwise the disappearance pattern of solar ν_e (atmospheric ν_μ) would remain unexplained. Moreover, if it were $\nu_4 \sim \nu_\tau$, then the triplet (ν_1, ν_2, ν_3) would approximately be a linear combination of (ν_μ, ν_e, ν_s), and thus the atmospheric ν_μ oscillation partner should be either ν_e (excluded) or ν_s (disfavored at $\gtrsim 99\%$ C.L.) or a linear combination of ν_e and ν_s (presumably disfavored). Therefore, the favored option for 3+1 spectra seems to imply $\nu_4 \sim \nu_s$, with (at least) a small subdominant component of ν_μ and ν_e in ν_4, necessary to drive LSND oscillations (see also [12,39]).[3]

Assuming $\nu_4 \sim \nu_s$ in 3+1 models, the triplet states (ν_1, ν_2, ν_3) would then approximately be linear combinations of $(\nu_e, \nu_\mu, \nu_\tau)$, and the triplet phenomenology of solar and atmospheric neutrinos would practically become equivalent to that of a standard framework with three active neutrinos. Such 3ν framework has been worked out in detail in previous papers [32,33,41], where the reader can find the corresponding constraints on the mass-mixing parameters. In conclusion, it seems that the emerging mixing pattern for the 3+1 spectrum implies, up to small ''LSND perturbations,'' an effective three-neutrino phenomenology for solar and atmospheric oscillations. In this case, it becomes important to study how well one can experimentally discriminate such 4ν option from pure 3ν oscillations.

VIII. SUMMARY AND CONCLUSIONS

In the context of 2+2 neutrino models, we have thoroughly analyzed the SK atmospheric data on the zenith distributions of lepton events, assuming the coexistence of both $\nu_\mu \to \nu_\tau$ and $\nu_\mu \to \nu_s$ oscillations, with a smooth interpolation between such two subcases. We have shown that, although the data disfavor oscillations in the pure $\nu_\mu \to \nu_s$ channel, one cannot exclude their presence *in addition* to $\nu_\mu \to \nu_\tau$ oscillations. High energy muon data appear to be crucial to assess the relative amplitude of the active and sterile oscillation channels for atmospheric neutrinos. We have also shown, in a qualitative way, that mixed active+sterile oscillations of atmospheric neutrinos are compatible with analogous oscillations of solar neutrinos, with different mixing pattern emerging from different choices for the solar ν solutions. Such results indicate that the solar and atmospheric neutrino phenomenology cannot be simply embedded in the usual two-family scenarios involving oscillations into either pure active or pure sterile states, and call for an extended 4ν framework involving combined solutions. Further directions to improve and constrain our present results might involve, on the one hand, a quantitative, global analysis of *world* neutrino oscillation data and, on the other hand, the inclusion of non-oscillatory data which have not been considered in this work, such as those coming from astrophysics and cosmology, and from direct neutrino mass measurements.

ACKNOWLEDGMENTS

E.L. thanks the organizers of the 19th International Conference on Neutrino Physics and Astrophysics (Sudbury, Canada), where preliminary results of this work were presented, for kind hospitality. We thank C. Giunti, R. Foot, T. Kajita, D. Montanino, M. Messier, R. Mohapatra, D. Petyt, F. Ronga, F. Vissani, and O. Yasuda for useful discussions or comments. This work was co-financed by the Italian Ministero dell'Università e della Ricerca Scientifica e Tecnologica (MURST) within the ''Astroparticle Physics'' project.

[3]Alternative 3+1 models with small (ν_s, ν_4) mixing are currently being investigated, see [40].

[1] S. M. Bilenky, C. Giunti, and W. Grimus, in *Proceedings of Neutrino '96*, Helsinki, 1996, edited by K. Enqvist *et al.* (World Scientific, Singapore, 1997), p. 174, hep-ph/9609343; V. Barger, S. Pakvasa, T. J. Weiler, and K. Whisnant, Phys. Rev. D **58**, 093016 (1998). For pre-LSND $2+2$ models, see also D. O. Caldwell and R. N. Mohapatra, *ibid.* **48**, 3259 (1993); J. T. Peltoniemi and J. W. F. Valle, Nucl. Phys. **B406**, 409 (1993).

[2] S. M. Bilenky, C. Giunti, and W. Grimus, Prog. Part. Nucl. Phys. **43**, 1 (2000).

[3] D. Dooling, C. Giunti, K. Kang, and C. W. Kim, Phys. Rev. D **61**, 073011 (2000).

[4] V. Barger and K. Whisnant, in *Current Aspects of Neutrino Physics*, edited by D. Caldwell (Springer-Verlag, Hamburg, 2000), hep-ph/0006235.

[5] LSND Collaboration, C. Athanassopoulos *et al.*, Phys. Rev. Lett. **81**, 1774 (1998); Phys. Rev. C **58**, 2489 (1998).

[6] LSND Collaboration, G. Mills, in ''Neutrino 2000,'' 19th International Conference on Neutrino Physics and Astrophysics Sudbury, Canada, 2000 (to be published), transparencies available at the site http://nu2000.sno.laurentian.ca

[7] Super-Kamiokande Collaboration, H. Sobel, in ''Neutrino 2000'' [6].

[8] Super-Kamiokande Collaboration, S. Fukuda *et al.*, Phys. Rev. Lett. **85**, 3999 (2000).

[9] Super-Kamiokande Collaboration, Y. Suzuki, in ''Neutrino 2000'' [6].

[10] MACRO Collaboration, B. Barish, in ''Neutrino 2000'' [6].

[11] C. Gonzalez-Garcia, in ''ICHEP 2000,'' 30th International Conference on High Energy Physics, Osaka, Japan, 2000, (to be published), transparencies available at the site http://www.ichep2000.rl.ac.uk

[12] V. Barger, B. Kayser, J. Learned, T. Weiler, and K. Whisnant, Phys. Lett. B **489**, 345 (2000).

[13] C. Giunti, M. C. Gonzalez-Garcia, and C. Peña-Garay, Phys. Rev. D **62**, 013005 (2000).

[14] For an update of the results discussed in [13], see M. C. Gonzalez-Garcia and C. Peña-Garay, hep-ph/0009041.

[15] G. L. Fogli, E. Lisi, and A. Marrone, in ''Neutrino 2000'' [6].

[16] O. Yasuda, hep-ph/0006319.

[17] B. Pontecorvo, Zh. Éksp. Teor. Fiz. **53**, 1717 (1967) [Sov. Phys. JETP **26**, 984 (1968)]; Z. Maki, M. Nakagawa, and S. Sakata, Prog. Theor. Phys. **28**, 675 (1962).

[18] L. Wolfenstein, Phys. Rev. D **17**, 2369 (1978); S. P. Mikheyev and A. Yu. Smirnov, Yad. Fiz. **42**, 1441 (1985) [Sov. J. Nucl. Phys. **42**, 913 (1985)]; Nuovo Cimento Soc. Ital. Fis., C **9**, 17 (1986); V. Barger, K. Whisnant, S. Pakvasa, and R. J. N. Phillips, Phys. Rev. D **22**, 2718 (1980).

[19] A. Yu. Smirnov, in ''Neutrino 2000'' [6].

[20] CDHSW Collaboration, F. Dydak *et al.*, Phys. Lett. **134B**, 281 (1984).

[21] D. O. Caldwell, G. M. Fuller, and Y.-Z. Qian, Phys. Rev. D **61**, 123005 (2000).

[22] N. Okada and O. Yasuda, Int. J. Mod. Phys. A **12**, 3669 (1997).

[23] S. M. Bilenky, C. Giunti, W. Grimus, and T. Schwetz, Astropart. Phys. **11**, 413 (1999).

[24] S. M. Bilenky, C. Giunti, B. Kayser, and S. T. Petcov, Phys. Lett. B **465**, 193 (1999).

[25] H. V. Klapdor-Kleingrothaus, H. Päs, and A. Yu. Smirnov, in *Beyond the Desert '99*, Proceedings of the 2nd International Conference on Physics Beyond the Standard Model: Accelerator, Nonaccelerator and Space Approaches, Tegernsee, Germany, 2000, edited by H. V. Klapdor-Kleingrothaus and I. V. Krivosheina (Bristol, IOP, 2000), hep-ph/9910205.

[26] A. Kalliomaki and A. Maalampi, Phys. Lett. B **484**, 64 (2000).

[27] E. Lisi, S. Sarkar, and F. L. Villante, Phys. Rev. D **59**, 123520 (1999).

[28] S. Esposito, G. Mangano, G. Miele, and O. Pisanti, J. High Energy Phys. **09**, 038 (2000).

[29] R. Foot and R. R. Volkas, Phys. Rev. D **55**, 5147 (1997).

[30] P. Di Bari and R. Foot, Phys. Rev. D **63**, 043008 (2001).

[31] V. Barger, Y. B. Dau, K. Whisnant, and B. L. Young, Phys. Rev. D **59**, 113010 (1999).

[32] G. L. Fogli, E. Lisi, A. Marrone, and G. Scioscia, Phys. Rev. D **59**, 033001 (1999).

[33] G. L. Fogli, E. Lisi, and D. Montanino, Phys. Rev. D **54**, 2048 (1996).

[34] F. Vissani and A. Yu. Smirnov, Phys. Lett. B **432**, 376 (1998); L. J. Hall and H. Murayama, *ibid.* **436**, 323 (1998).

[35] E. Akhmedov, P. Lipari, and M. Lusignoli, Phys. Lett. B **300**, 128 (1993); P. Lipari and M. Lusignoli, Phys. Rev. D **58**, 073005 (1998); Q. Y. Liu and A. Yu. Smirnov, Nucl. Phys. **B524**, 505 (1998); Q. Y. Liu, S. P. Mikheyev, and A. Yu. Smirnov, Phys. Lett. B **440**, 319 (1998); R. Foot, R. Volkas, and O. Yasuda, Phys. Rev. D **58**, 013006 (1998).

[36] Particle Data Group, D. E. Groom *et al.*, Eur. Phys. J. C **15**, 1 (2000).

[37] A. Geiser, in ''Neutrino 2000'' [6].

[38] D. Petyt, ''$\nu_\mu \to \nu_s$ in MINOS,'' MINOS internal note NuMI-L-691, available at www.hep.anl.gov/ndk/hypertext/numi_notes.html

[39] O. L. G. Peres, talk at ''NOW 2000,'' 2nd Europhysics Neutrino Oscillation Workshop, (Conca Specchiulla, Otranto, Lecce, Italy, 2000, transparencies available at www.ba.infn.it/~now2000; O. L. G. Peres and A. Yu. Smirnov, hep-ph/0011054.

[40] C. Giunti, talk at ''NOW 2000''; C. Giunti and M. Laveder, hep-ph/0010009.

[41] G. L. Fogli, E. Lisi, D. Montanino, and G. Scioscia, Phys. Rev. D **55**, 4385 (1997); G. L. Fogli, E. Lisi, and A. Marrone, *ibid.* **57**, 5893 (1998); G. L. Fogli, E. Lisi, D. Montanino, and A. Palazzo, *ibid.* **62**, 013002 (2000); **62**, 113004 (2000).